# Characteristic Spectrum of Very Low-Energy Photoelectron from Above-Threshold Ionization in the Tunneling Regime

C. Y. Wu,[*] Y. D. Yang, Y. Q. Liu, and Q. H. Gong[†]

*State Key Laboratory for Mesoscopic Physics, Department of Physics, Peking University, Beijing 100871, China*

M. Wu and X. Liu

*State Key Laboratory of Magnetic Resonance and Atomic and Molecular Physics, Wuhan Institute of Physics
and Mathematics, Chinese Academy of Sciences, Wuhan 430071, China*

X. L. Hao and W. D. Li

*Institute of Theoretical Physics and Department of Physics, Shanxi University, 030006 Taiyuan, China*

X. T. He and J. Chen[‡]

*HEDPS, Center for Applied Physics and Technology, Peking University, Beijing 100084, China*
*Institute of Applied Physics and computational Mathematics, P.O. Box 8009, Beijing 100088, China*

We report an experimental and theoretical study of very low-energy photoelectrons in tunneling ionization process from noble gas atoms interacting with ultrashort intense infrared laser pulses. A universal peak structure with electron energy well below 1 eV in the photoelectron spectrum, corresponding to the double-hump structure in the longitudinal momentum distribution, is identified experimentally for all atomic species. Our quantum and semiclassical analysis reveal the role of long-range Coulomb potential in the production of this very low-energy peak structure.

Since its first observation in 1979 [1], above-threshold ionization (ATI) has been a fundamental process that plays an essential role in understanding the intense laser-matter interaction [2]. In the tunneling regime where the Keldysh parameter $\gamma = \sqrt{I_p/2U_p} \ll 1$ (where $I_p$ is the ionization potential and $U_p = F_0^2/(2\omega)^2$ the ponderomotive energy, $\omega$ the laser angular frequency and $F_0$ the peak amplitude of the laser field) [3], the ATI spectrum was expected to be consistent with the Simpleman's picture originating from the semiclassical viewpoint of the atom-laser interaction [4]. The overall spectrum drops fast from the origin until $2U_p$ where a flat plateau emerges and extends to a cutoff at $10U_p$, which can be well explained by a rescattering process [5,6].

In contrast to the prediction of the standard tunneling picture, it was discovered that low-energy photoelectrons in the ATI process possess nontrivial behavior. For example, the low-energy momentum distribution of photoelectrons shows some intriguing structures deviating obviously from the Simpleman's perspective [7,8], which has been intensively investigated recently and its mechanism is still in debate [9–14]. More recently, a peculiar low-energy structure (LES) has been found in ATI spectra in the tunneling regime [15,16], which is also in striking contrast to the prediction of the Simpleman's model. Semiclassical model [16–18] has been applied to explore this low-energy structure and revealed the essential role of the long range Coulomb potential in its production.

Moreover, significant effect of the Coulomb potential on the low-energy photoelectron dynamics has also been explored in near-threshold high harmonic generation [19].

At present, there are still several puzzles in the low-energy ATI spectrum. One is that although the two experimental observations agree on the LES with electron energies above 1 eV [15,16], Ref. [16] reports a sharp peak structure, or very-low-energy structure (VLES), which is well below 1 eV and depends hardly on the laser wavelength and intensity. In contrast, this VLES was not found in Ref. [15]. The other one concerns the relationship between the LES and the particular structure in the momentum distribution [8,12,13], as both of them are related to the dynamics of low-energy photoelectron. Therefore, the dynamics of photoelectron in ATI process, especially the low-energy electron, is still far from being fully understood, even though ATI process has been studied for more than thirty years since its first observation [1]. In this Letter, we aim to resolve these puzzles and perform a comprehensive analysis on the dynamics of photoelectron with very low energy (< 1 eV) in the tunneling regime.

The experiments were performed using a newly built cold target recoil-ion momentum spectroscopy (COLTRIMS) [20]. A commercial multipass femtosecond amplifier (Femtolasers GmbH) delivers laser pulses with a central wavelength of ∼800 nm and pulse duration of 24 fs at a repetition rate of 3 kHz. An optical parametric amplifier (OPA, TOPAS-C, Light Conversion, Inc.) is used to

generate wavelength-tunable midinfrared femtosecond laser pulses. The pulse durations are ~30 fs at 1320 nm and ~60 fs at 1800 nm. The laser beam was then tightly focused on the collimated supersonic gas jet in an ultrahigh vacuum chamber ($\sim 5 \times 10^{-11}$ mbar). Electrons and ions thus generated were accelerated by applying weak homogenous electric (3 V/cm) and magnetic ($\sim 5$ G) fields and recorded by two opposite position-sensitive delay-line detectors (Roentdek Handels GmbH). From the time of flight and position on the detectors the momentum vectors of electrons and ions were calculated. The momentum resolution is ~0.02 a.u. along the laser polarization direction. In particular, we employ the electron-ion momentum conservation in the data analysis to ensure that the electrons are generated from the single ionization of the gas targets.

Figs. 1(a)–1(c) show the low-energy part of the measured photoelectron spectra (collected in a solid angle of 5–8 degrees in the field direction) of noble gas atoms at different laser wavelengths and intensities. The parameters chosen here guarantee that the process is in the tunneling regime ($\gamma < 1$) and $I_p/\omega \gg 1$ to suppress the resonance channel in the ionization process. Several ATI peaks can be clearly seen in the spectrum for wavelength of 800 nm. With increasing wavelength, the ATI peaks become less pronounced and can be hardly distinguished in the spectrum for 1800 nm. On the other hand, the LES [15,16] becomes noticeable in the long-wavelength spectra. We will denote this as the high-energy low-energy structure (HLES) throughout this Letter, in order to distinguish it from the very-low-energy structure. (For visual convenience, the HLES and the VLES are marked by dashed and solid arrows, respectively, in all figures of energy spectra in this Letter). It is intriguing that all spectra
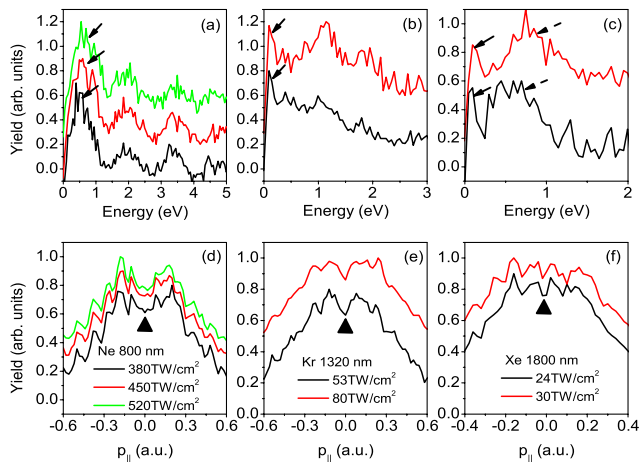
show a VLES below 1 eV, which is located at about 0.5 eV for 800 nm and 0.1–0.2 eV for 1320 nm and 1800 nm, respectively.

For comparison, longitudinal momentum distributions (LMD) corresponding to the ATI spectra, which are obtained by integrating over all transverse momenta of the photoelectrons, are depicted in Figs. 1(d)–1(f). It is noteworthy that all distributions show the profile of a double-hump structure (DHS): a central minimum with a pronounced hump on each side that consists of a series of peaks. For 800 nm, this structure reproduces the result presented by Rudenko *et al.* [12]. In addition, it can be found that the humps on either side of the central minimum correspond to the VLES in the energy spectrum. For 800 nm, for example, the hump in the momentum distribution locates at about 0.2 a.u., corresponding to the peak at about 0.5 eV in the energy spectrum. This DHS in the LMD can be qualitatively reproduced in the semiclassical simulation [7,9], *S*-matrix calculation [11,14], and numerical solution of three-dimensional time-dependent Schrödinger equation (TDSE) [10,21]. However, its underlying mechanism has not been fully explored.

To reveal the underlying mechanism of these structures, we calculate the spectrum of Xe atom using a three-dimensional TDSE code [22] (In our calculation, the laser parameters are the same as those in the experiment and a Gaussian envelop is assumed for the pulse shape). As shown in Figs. 2(a) and 2(b), TDSE calculation with focal average qualitatively reproduces the experimental observation: a VLES well below 1 eV in the ATI spectrum and a DHS in the LMD. For comparison, calculations with a short-range ion potential and a hydrogen-like potential are also presented in Fig. 2. It is noteworthy that, for short-range potential, the structures in the ATI spectrum, including both the HLES and the VLES, disappear and accordingly the LMD shows a central peak distribution [see Fig. 2(b)], indicating that the long-range Coulomb potential plays an essential role in the dynamics of low-energy photoelectron in ATI [10,21]. On the other



FIG. 1 (color online).   Low-energy photoelectron energy spectra and longitudinal momentum distributions of Ne [(a),(d)], Kr [(b),(e)], and Xe [(c),(f)] in infrared laser fields. For visual convenience, the VLES and HLES are marked by solid and dashed arrows in all figures of energy spectrum, respectively (see text).
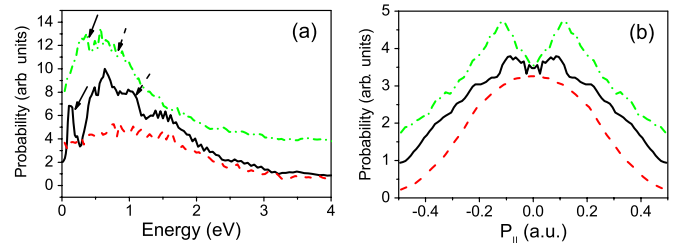


FIG. 2 (color online).   Low-energy photoelectron energy spectrum (a) and longitudinal momentum distribution (b) calculated using numerical solution of TDSE for Xe (black solid line) and short-range potential (red dashed line). Calculated result using a hydrogen-like potential with the same ground state energy of Xe is also shown (green dash-dotted line) (see text). $I = 3 \times 10^{13}$ W/cm² and $\lambda = 1800$ nm.

side, the results with a hydrogen-like potential are quali-
tatively consistent with the experimental observation.
However, a more pronounced central minimum in the
momentum distribution [Fig. 2(b)] has been found in the
calculations than that in the experimental data, which will
be further discussed later.

To gain further insight into these peculiar structures,
we compare the experimental data with the result of the
theoretical simulation based on a semiclassical description
of the ionization process. Details of the semiclassical
approach have been described elsewhere [23]. In brief,
we consider model atoms with hydrogen-like potentials
of $V = -Z_{\mathrm{eff}}/r$ (where $Z_{\mathrm{eff}}$ is the effective nuclear charge
to give ground state energy equal to that of corresponding
atoms) interacting with an external laser field. The laser
field $\epsilon(t) = f(t)E_0 \cos\omega t$ has a constant amplitude for
the first ten cycles and is ramped off within 3 cycles.
For simplification, the electron is released within the
time interval $-\pi/2 \le \omega t \le \pi/2$ through tunneling with
a rate given by the Ammosov-Delone-Krainov formula
[24]. The subsequent evolution of the electron is deter-
mined by the Newton's equation of motion.

The simulation results are shown in Fig. 3 and exhibit
the following main features: all energy spectra show a
VLES below 1 eV and a HLES, which develops and shifts
with intensity; the position of the VLES locates at about
0.5 eV and shifts slightly with intensity for 800 nm, while
for 1320 and 1800 nm, it locates at about 0.1 eV indepen-
dently of intensity; all LMDs show a DHS and, on each
side, the hump consists of one pronounced peak at low
intensity or two or more peaks at high intensity; the peaks
beside the minimum in the LMD correspond to the VLES
in the ATI spectrum. Clearly, the main features shown in
the semiclassical simulation are qualitatively consistent
with the experimental results.

In order to shed more light on the physical picture
behind, we further calculate the two-dimensional electron
momentum distributions (2dMD). As shown in Figs. 4(a)
and 4(b), besides a shift of both the direct electron and
indirect electron [25] to the opposite direction of the
tunneling exit of the electron due to the Coulomb potential
[16], the total 2dMD [Fig. 4(c)] shows some more par-
ticular structures. A dense lump structure (DLS) locating
below $p_{\parallel} = 0.2$ a.u. [region inside a black solid pane in
Fig. 4(c)] followed by a hatlike structure [region inside a
blue dotted pane in Fig. 4(c)] appears near the z axis (field
direction). In addition, two strips, with electron momenta
$p_{\parallel}$ of roughly 0.07 and 0.17 a.u., extend out in the direction
almost perpendicular to the field direction. The DLS and
strip structures in 2dMD [Fig. 4(c)] give rise to DHS in
LMD [Fig. 3(e)]. Moreover, the VLES and HLES in
Fig. 3(b) correspond to the DLS and hat-like structure in
Fig. 4(c), respectively.

Comparing Fig. 4(c) with Figs. 4(a) and 4(b), one
can see that the position of the DLS corresponds to the
positions of the lower boundary of the indirect electrons
and the upper boundary of the direct electrons in the



FIG. 3 (color online).   Low-energy photoelectron energy spec-
tra and longitudinal momentum distributions of atoms calculated
using semiclassical model. (a),(d) Ne. $\lambda = 800$ nm; (b),(e) Kr.
$\lambda = 1320$ nm; (c),(f) Xe. $\lambda = 1800$ nm.
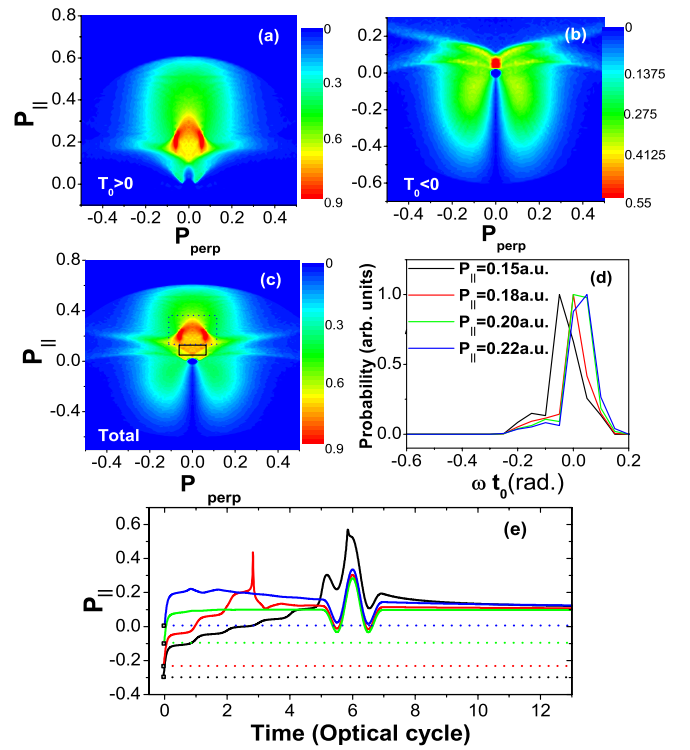


FIG. 4 (color online).   (a)–(c) Calculated two-dimensional
electron momentum distributions for Kr (z is the laser polariza-
tion direction). $I = 8 \times 10^{13}$ W/cm$^2$ and $\lambda = 1320$ nm. See the
text for the details. (d) Distributions of the initial tunnel-
ionization phase ($\omega t_0$) of the electron with the corresponding
final drift momentum in the field direction. (e) Temporal evolu-
tion of drift momenta of four trajectories with different initial
conditions with (solid line) and without (dotted line) Coulomb
potential.

2dMD, indicating that the DHS is closely related to the shift due to the Coulomb potential. This is partly consistent with the analysis of Dimitriou *et al.* [9]. Moreover, as shown in Figs. 1 and 3, the prominent HLES in the energy spectrum is hardly distinguished while the VLES still manifests in the LMD. This is because the HLES is mainly due to the Coulomb focusing effect [16–18]; integration over the transverse momentum mostly smears out this effect. In contrast, the DHS will not be spoiled by the integration since it partly comes from the shift due to the Coulomb potential.

Moreover, it deserves noting that the DLS and other structures, e.g., the strips shown in Fig. 4(c) cannot be only attributed to Coulomb distortion since distortion can only give rise to a smooth distribution with a shifted maximum in the LMD. This point can be clearly seen in Fig. 4(d) that shows the distributions of the initial tunnel-ionization phase ($\omega t_0$) of the electron with the corresponding final drift momentum in the field direction. In general, the phase increases with momentum and the averaged phase of the electron with $P_\parallel$ in the range from 0.15 to 0.22 a.u. is at about $\omega t_0 = 0$, which is in agreement with the distortion picture [9]. However, the phase distributions exhibit a distinct overlap for different longitudinal momenta, indicating that the interaction between the electron and the ion core significantly redistributes the electron momentum. This can be further demonstrated by Fig. 4(e), which shows the evolution of the longitudinal momenta of electron trajectories with different initial conditions (i.e., with different tunnel ionization time and transverse momenta). Without the Coulomb potential, the electrons' final longitudinal momenta are solely determined by the initial tunnel ionization time $t_0$ [$p = -A(t_0)$ where $A(t)$ is the vector potential of the laser field] and are quite different. In contrast, all of them develop an identical momentum and contribute to the DLS at about 0.1–0.2 a.u. in the 2dMD [Fig. 4(c)] with Coulomb potential considered. Moreover, this picture also applies to the strip structures in Fig. 4(c). In Fig. 4(e), abrupt changes of the drift momenta indicate strong interaction of the electrons with the Coulomb potential when they return to the core. Note that this strong interaction does not require a very close approaching of the electron to the ion [26] since the electron with initial phase $\omega t \sim 0$ considered here returns to the core with very low kinetic energy. It is worth mentioning that the mechanism revealed here for the VLES is similar to an electron energy bunching process discussed in Ref. [27].

It is noteworthy that, by comparing Fig. 3 with Fig. 4, the VLES in the energy spectrum for long wavelengths (1320 nm and 1800 nm) more likely corresponds to the first hump beside the minimum but not the second hump in the LMD since the energy spectrum is obtained by integrating over a small solid angle (5–8 degree) around the field direction and the LMD is obtained by integrating the total transverse momentum. However, for the 800 nm case

with much higher intensities, the most apparent humps locate at larger momenta [about $\pm 0.2$ a.u., see Fig. 3(d)] in the momentum distribution. As a consequence, the VLES shifts to a higher energy position. All these features are consistent with the experimental observations.

A closer inspection, however, reveals some discrepancies between the semiclassical and experimental spectra. This can be attributed to the quantum nature of the process, which is obviously neglected in the semiclassical model. One is that the ATI structure shown in Figs. 1(a) and 1(b), corresponding to absorption of integral number of photons, is absent in the semiclassical spectrum. In fact, these ATI peaks tend to smear out the classical effects shown in Fig. 3. The HLES in the energy spectrum [Fig. 3(a)] is hardly distinguishable in Fig. 1(a) [28]. In addition, the fine structure (multiple humps developed at high intensity) in the LMD is also hardly distinguishable in the experimental result. However, the DHS in Fig. 3(d) is qualitatively consistent with the experiment in spite of disturbance from the ATI peaks visible in Fig. 1(d). Furthermore, the energy peak at about 0.5 eV, which appears as an ATI peak in Fig. 1(a) and corresponds to the DHS in the LMD, can be considered to correspond to the VLES shown in Fig. 3(a) since these structures are absent in both TDSE and semiclassical simulations for short-range potential (not shown here). Moreover, this quantum nature of the process, which tends to spoil the visibility of the classical effect, diminishes with increasing wavelength, which is clearly shown by the fact that the experimental result is more consistent with the semiclassical simulation at longer wavelengths.

The other discrepancy is that the minimum in the semiclassical LMD is more pronounced than the experimental data and TDSE simulation for Kr and Xe, which can be attributed to two effects. One is that the classical treatment overestimates the probability of electrons with very low return energy being trapped by the Coulomb potential, resulting in the suppression of the electron spectrum near the origin [7]. Another one is that Freeman-resonance effect, which is absent in the semiclassical simulation, still play a noticeable role here. It has been demonstrated that the resonance process will largely affect the ATI spectrum, especially the longitudinal momentum distribution, even in the tunneling regime [13,21]. Under the laser intensities achieved in our experiment at longer wavelengths, the resonance channel can still have an important contribution due to abundant excited states in Kr and Xe atoms [29], resulting in a less prominent DHS shown in Figs. 1(e) and 1(f). This point can be seen by the fact that the spectra, especially the momentum distribution, are much more close to the experimental result when a model potential, which faithfully reproduces the energy-level structure of Xe, is used in the TDSE calculations (see Fig. 2), comparing with that of a hydrogen-like potential, which shows a deep central minimum in the momentum distribution.

In summary, we report experimental and theoretical studies on very low-energy ATI photoelectron in the tunneling ionization process. The COLTRIMS measurement reveals a universal peak structure below 1 eV in the energy spectrum, which corresponds to a double-hump structure in the longitudinal momentum distribution for all noble gas atomic species. These structures can be qualitatively reproduced in quantum and semiclassical simulations. Our analysis reveals the role of the long-range Coulomb potential in the origin of these particular structures.

---

*cywu@pku.edu.cn

†qhgong@pku.edu.cn

‡chen_jing@iapcm.ac.cn

[1] P. Agostini, F. Fabre, G. Mainfray, G. Petite, and N. K. Rahman, Phys. Rev. Lett. **42,** 1127 (1979).

[2] For a review, see, e.g., W. Becker, F. Grasbon, R. Kopold, D. B. Miloševi, G. G. Paulus, and H. Walther, Adv. At. Mol. Opt. Phys. **48,** 35 (2002).

[3] L. V. Keldysh, Zh. Eksp. Teor. Fiz. **47,** 1945 (1964); [Sov. Phys. JETP **20,** 1307 (1965)].

[4] H. B. van Linden van den Heuvell and H. G. Muller, *Multiphoton Processes*, edited by S. J. Smith and P. L. Knight (Cambridge University Press, Cambridge, England, 1988), p. 25.

[5] P. B. Corkum, N. H. Burnett, and F. Brunel, Phys. Rev. Lett. **62,** 1259 (1989); P. B. Corkum, Phys. Rev. Lett. **71,** 1994 (1993).

[6] G. G. Paulus, W. Nicklich, H. Xu, P. Lambropoulos, and H. Walther, Phys. Rev. Lett. **72,** 2851 (1994).

[7] J. Chen and C. H. Nam, Phys. Rev. A **66,** 053415 (2002).

[8] R. Moshammer *et al.*, Phys. Rev. Lett. **91,** 113002 (2003).

[9] K. I. Dimitriou, D. G. Arbo, S. Yoshida, E. Persson, and J. Burgdorfer, Phys. Rev. A **70,** 061401(R) (2004).

[10] Z. Chen, T. Morishita, A.-T. Le, M. Wickenhauser, X.-M. Tong, and C. D. Lin, Phys. Rev. A **74,** 053405 (2006).

[11] L. Guo, J. Chen, J. Liu, and Y. Q. Gu, Phys. Rev. A **77,** 033413 (2008).

[12] A. Rudenko, K. Zrost, C. D. Schröter, V. L. B. de Jesus, B. Feuerstein, R. Moshammer, and J. Ullrich, J. Phys. B **37,** L407 (2004).

[13] A. S. Alnaser, C. M. Maharjan, P. Wang, and I. V. Litvinyuk, J. Phys. B **39,** L323 (2006).

[14] F. H. M. Faisal and G. Schlegel, J. Phys. B **38,** L223 (2005); J. Mod. Opt. **53,** 207 (2006).

[15] C. I. Blaga, F. Catoire, P. Colosimo, G. G. Paulus, H. G. Muller, P. Agostini, and L. F. DiMauro, Nature Phys. **5,** 335 (2009).

[16] W. Quan *et al.*, Phys. Rev. Lett. **103,** 093001 (2009).

[17] C. P. Liu and K. Z. Hatsagortsyan, Phys. Rev. Lett. **105,** 113003 (2010).

[18] T. Yan, S. V. Popruzhenko, M. J. J. Vrakking, and D. Bauer, Phys. Rev. Lett. **105,** 253002 (2010).

[19] D. C. Yost, T. R. Schibli, J. Ye, J. L. Tate, J. Hostetter, M. B. Gaarde, and K. J. Schafer, Nature Phys. **5,** 815 (2009); E. P. Power, A. M. March, F. Catoire, E. Sistrunk, K. Krushelnick, P. Agostini, and L. F. DiMauro, Nature Photon. **4,** 352 (2010).

[20] Y. Liu, X. Liu, Y. Deng, C. Wu, H. Jiang, and Q. Gong, Phys. Rev. Lett. **106,** 073004 (2011).

[21] M. Abu-samha and L. B. Madsen, J. Phys. B **41,** 151001 (2008); M. Abu-samha, D. Dimitrovski, and L. B. Madsen, J. Phys. B **41,** 245601 (2008).

[22] J. Chen, B. Zeng, X. Liu, Y. Cheng, and Z. Z. Xu, New J. Phys. **11,** 113021 (2009). In our calculation under single-active-electron approximation for Xe, a model potential that can faithfully reproduce the energy-level structure of Xe is used.

[23] B. Hu, J. Liu, and S. G. Chen, Phys. Lett. A **236,** 533 (1997); J. Chen, J. Liu, and S. G. Chen, Phys. Rev. A **61,** 033402 (2000); J. Chen, J. Liu, and W. M. Zheng, Phys. Rev. A **66,** 043410 (2002); D. F. Ye, X. Liu, and J. Liu, Phys. Rev. Lett. **101,** 233003 (2008).

[24] N. B. Delone and V. P. Krainov, J. Opt. Soc. Am. B **8,** 1207 (1991).

[25] Here direct and indirect electrons imply the electrons those are tunnel-ionized in the rising edge ($\omega t \epsilon [-\pi/2, 0]$) and the falling edge ($\omega t \epsilon [0, \pi/2]$), respectively. To reduce the calculations, we have restricted the initial phase intervals to the interval $\omega t \epsilon [-\phi, 0]$ and $[0, \phi]$ where $\phi$ is given a value such that the final kinetic energy of the electron ionized in these initial phase intervals satisfies $E_k < 2$ eV when the Coulomb potential is absent.

[26] The distance between the electron and the ion core is usually $\gtrsim 10$ a.u. according to our calculation.

[27] A. Kästner, U. Saalmann, J. M. Rost, Phys. Rev. Lett. **108,** 033201 (2012).

[28] The HLES can be roughly distinguished in large scale energy spectrum of He for 800 nm at intensity of $4$–$6 \times 10^{14}$ W/cm$^2$. P. Agostini (private communication).

[29] C. M. Maharjan, A. S Alnaser, I. Litvinyuk, P. Ranitovic, and C. L. Cocke, J. Phys. B **39,** 1955 (2006).